NJC

PAPER

View Article Online
View Journal

Cite this: DOI: 10.1039/c7nj00564d

Synthesis of porous polymeric metalloporphyrins for highly efficient oxidation of cyclohexane in heterogeneous systems†

Yongjin Li, Chuanrong Liu and Weijun Yang *

Received 16th February 2017,
Accepted 26th June 2017

DOI: 10.1039/c7nj00564d

rsc.li/njc

Herein, porphyrin-conjugated organic polymers, Mn(III)P-CMP and Fe(III)P-CMP, were synthesized by Suzuki coupling reaction with manganese/iron tetraphenylporphyrin (T(p-Br)PPMn/FeCl) and 1,4-phenyldiboronic acid as building blocks. The structures of the pore and surface were characterized by nitrogen adsorption and desorption isotherm, FE-SEM, and HR-TEM. The electrochemical behavior of Mn(III)P-CMP was tested by cyclic voltammetry. For the catalytic oxidation of higher inert C–H bond in cyclohexane, Mn(III)P-CMP and Fe(III)P-CMP with hyper-conjugated and microporous structures functioned better than the monomer metalloporphyrin. With MnP-CMP as the preferred catalyst, after 3.5 h of reaction, the yield of cyclohexanol and cyclohexanone was 21.6%, and the conversion of cyclohexane reached 29.9% at the Mn^{3+}/cyclohexane molar ratio of 1/168 000, 150 °C, and 0.8 MPa. Mn(III)P-CMP and Fe(III)P-CMP were structurally stable and insoluble in common solvents and hardly degraded below 300 °C; hence, they had excellent reusability.

1. Introduction

Owing to its industrial importance, the oxidation of cyclohexane to corresponding products has been investigated for decades, and some meaningful research results have been achieved.[1–4] Cytochrome P450 can efficiently activate oxygen molecules for the highly selective catalytic oxidation of the C–H bond to form corresponding products under mild conditions.[5,6] Metalloporphyrin, which has a structure similar to that of the active center of cytochrome P450 enzyme, also functions similarly and is green, efficient, environmentally friendly, and reactive under mild conditions.[7–10] Tetraphenylmetalloporphyrin has been used as a biomimetic catalyst for the catalytic oxidation of cyclohexane, which elevates the conversion rate of cyclohexane from 4% to 10% with the reaction time reduced to half as compared to that under the original, non-catalytic conditions with cyclohexanol or cyclohexanone as additives. Moreover, the total selectivity of cyclohexanol and cyclohexanone is increased from 78% to 85% or higher.[11–13] However, metalloporphyrin can be easily degraded by the high concentration of peroxide produced in the reaction system; this causes the loss of oxidation activity and recyclability as well as considerable high cost in industrial application.[14,15]

The commonly used method to solve this problem is the immobilization of monomer metalloporphyrin on a solid support surface that converts metalloporphyrin catalytic system to heterogeneous catalysis.[16–18] On the one hand, it improved the stability of metalloporphyrin *via* the adsorption properties of porphyrin on different solid support surfaces. On the other hand, it also improved the catalytic efficiency of metalloporphyrin due to the intrinsic characteristics of solid support. However, the bond between porphyrin and solid support surface is not stable. In addition, the activity of the supported metalloporphyrin rapidly declines when it is reused.[19] This problem may be solved by aggregating metalloporphyrins into special insoluble macromolecular polymers.[20–24] Side chains outside the metalloporphyrin macrocycle are bridged by the groups with conjugated effect to form a hyper-conjugated micro–mesoporous polymer (CMP).[25–27] Recently, researchers have endeavoured to prepare CMPs with new structures.[28–30] Jiang *et al.* reported a Fe-based micro–mesoporous-conjugated porphyrin polymer that catalytically oxidized organic sulfur and olefin double bond compounds.[31,32] CMPs in which porphyrin monomers were connected with stable covalent bonds were superior to the supported porphyrin. The hyper-conjugated effect enhanced the stability of porphyrin, and the CMPs with micro–mesoporous and large surface area allowed more exposure of porphyrin active reaction sites on the surface of polymer, which clearly improved the catalytic efficiency. A series of phenylimine-bridged and alkynyl-bridged manganese porphyrin polymers was synthesized and applied to aerobic oxidation of alcohols and toluene in our previous works, which showed good catalytic activity.[33,34]

Department of Chemistry and Chemical Engineering, Hunan University, Changsha 410082, Hunan, China. E-mail: wjyang@hnu.edu.cn; Fax: +86 731 88713642; Tel: +86 731 88821449

† Electronic supplementary information (ESI) available. See DOI: 10.1039/c7nj00564d

Herein, the conjugated porous metalloporphyrin polymers FeP-CMP and MnP-CMP coupled with phenylene were synthesized using metalloporphyrin as the monomer and applied in the highly efficient catalytic oxidation of higher inert C–H bond in cyclohexane. Due to their high stability, FeP-CMP and MnP-CMP resisted the damages caused by high-concentration of cyclohexane peroxide and high temperature, such that the catalytic activities were retained, and the catalysts could be reused. Due to the synergistic effect of hyper-conjugation and numerous pores, the catalytic activities were found to be higher than those of monomer metalloporphyrin, and the selectivity of the target products alcohol and ketone augmented as well. Accordingly, CMPs are potentially eligible heterogeneous catalysts for cyclohexane oxidation.

2. Experimental

2.1. Reaction reagents and instruments

Bis(tricyclohexylphosphine)palladium(0), 1, 4-dioxane, 1,4-phenyldiboronic acid, and other reagents were analytical grade and purchased from J&K Chemicals, and 1,4-dioxane was distilled over benzophenone ketyl under argon before use. T(P-Br)PPMnCl and T(p-Br)PPFeCl were synthesized by our group according to the documented procedures and characterized by IR, UV-vis, ^{1}H-NMR, and MS spectroscopic methods (ESI†).[35]

The specific surface areas and pore size distribution were detected by Beckman Coulter, Inc. SA 3100 accelerated surface and porosity analyzer with nitrogen as the probing gas at 77 K. The specific surface areas were calculated by the Brunauer–Emmett–Teller (BET) method, and the NLDFT theory was utilized to estimate the pore size, pore volume, and pore distribution. Field emission scanning electron microscopy (FE-SEM) images were obtained using a JEOL model JSM-5600Lv microscope. Before measurements, gold was sprayed on the surface of the samples. High resolution transmission electron microscopy (HR-TEM) images were obtained using a JEOL model JEM-3010 microscope. FT-IR spectra were obtained using a Fourier transform infrared spectrometer (IRrestige-21, Shimadzu), and the sample was completely dried and diluted by potassium bromide. UV-vis absorption spectra were obtained using a Cary 100 UV-Vis spectrophotometer from Agilent technologies, and the diffuse reflectance spectra were obtained *via* the spectrophotometer equipped with integration sphere, and the sample was diluted with $BaSO_4$. Elemental analyses of C, H, and N were carried out using a vario ELIII model from German Elementar corporation. Elemental analyses of Mn/Fe were carried out by atomic absorption spectrometry using a Perkin Elmer Aanalyst 700/800. Elemental analyses of Br and Cl were carried out by combustion.

2.2. Synthesis of Fe and Mn porphyrin polymers

To connect porphyrin monomers to form polymers, we chose T(p-Br)PPMnCl and 1,4-phenyldiboronic acid with two boronates as building blocks in the presence of bis(tricyclohexylphosphine)-palladium(0) as the catalyst under alkaline condition to synthesize Mn(III)P-CMP by the Suzuki cross-coupling reaction (Fig. 1).

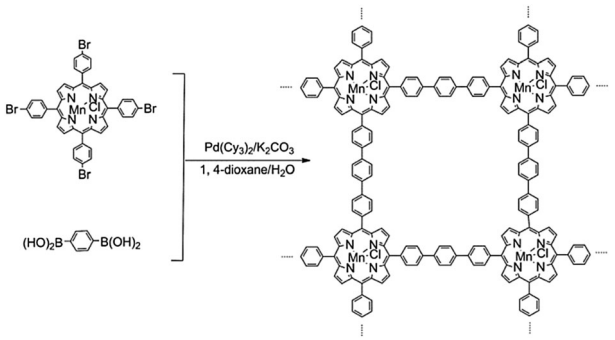

Fig. 1 Schematic of the MnP-CMP synthesis.

Mn(III)P-CMP was synthesized *via* the following steps: a mixture of T(p-Br)PPMnCl (0.20 mmol), K_2CO_3 (1.60 mmol), bis(tricyclohexylphosphine)palladium(0) (20 μmol), 1,4-phenyldiboronic acid (0.80 mmol), 1,4-dioxane (16.0 mL), and aqueous solution (4.0 mL) was added to a reaction flask, degassed by three freeze–pump–thaw cycles, purged with argon, and stirred at 125 °C for 24 h. TLC method was used to detect excess 1,4-phenyldiboronic acid. Finally, the mixture was allowed to cool at room temperature and poured into plenty of water. The precipitate was obtained by filtration, thoroughly washed with THF, methanol and trichloromethane, and then dried in vacuum. The solid was rigorously washed by Soxhlet extraction for 24 h with THF, methanol, and trichloromethane until the solvent in the Soxhlet extractor did not exhibit porphyrin peaks in UV-vis detection and then dried in vacuum to obtain Mn(III)P-CMP as dark green solid particles in 91.12% yield, Mn content: 4.98%. The synthesis method of Fe(III)P-CMP was the same as that of Mn(III)P-CMP, giving atroviren solid particles in 90.36% yield, Fe content: 4.22%.

2.3. Cyclic voltammetry of Mn(III)P-CMP

Cyclic voltammetry was performed using a CHI66OB electrochemical workstation with a three-electrode cell system in which a glassy carbon electrode after loading MnP-CMP, a calomel electrode, and a Pt wire were used as the working, reference, and counter electrodes, respectively. For the preparation of the working electrode, 6.0 mg of Mn(III)P-CMP sample was dispersed in 0.5 mL of solvent mixture containing 11 μL of Nafion (5 wt%) and 0.49 mL of ethanol by sonication for more than 1 h to obtain a stable suspension. Subsequently, 10 μL portion of the sample solution was slightly dropped on the surface of the pre-polished glassy carbon electrode. The electrodes were dried overnight at room temperature for measurement. The electrochemical experiments were conducted in 0.1 mol L^{-1} $(CH_3CH_2)_4NBr$ CH_2Cl_2 solution and cyclically scanned at a scan rate of 50 mV s^{-1} at room temperature after Ar gas was purged for 10 min.

2.4. Catalytic oxidation of cyclohexane

Cyclohexane oxidation with air was catalyzed by Mn(III)P-CMP. Cyclohexane 200 mL (1.85 mol) and Mn^{3+}/cyclohexane = 1/168 000 (molar ratio) of Mn(III)P-CMP were added to a 250 mL autoclave reactor. The stirring speed was set at 400 rpm, with the

needle valve and rotameter switch controlling and metering the gas flow rate, respectively. The mixture was rapidly sampled and analyzed during the reaction. Reaction products were identified by GC-MS (Shimadzu QP-5000 MS). The samples were analyzed by GC using chlorobenzene as an internal standard. Chromatographic analyses were conducted using a Shimadzu GC-17A series gas chromatograph (helium as the carrier gas) equipped with an FID detector and a PEG-20000 (25 m × 0.25 mm) capillary column. The contents of adipic acid, ester, and hyperoxide were measured by chemical titration according to a documented procedure.[36]

3. Results and discussion

3.1. Mn/FeP-CMP characterization

Mn(III)P-CMP and Fe(III)P-CMP conjugated metalloporphyrin polymers had large surface areas and porous structures. The BET surface areas of Mn(III)P-CMP and Fe(III)P-CMP were as high as 325 $m^2\ g^{-1}$ and 296 $m^2\ g^{-1}$, respectively (Table 1). Moreover, the BET surface area of the monomer metalloporphyrin powders was much lower than that of CMPs and almost without pores. Therefore, Mn(III)P-CMP is an excellent micro- and mesoporous polymer.

Table 1 Specific surface areas and pore volumes of Mn(III)P-CMP, Fe(III)P-CMP, and T(p-Br)PPMnCl

	S_{BET} ($m^2\ g^{-1}$)	S_{micro} ($m^2\ g^{-1}$)	V_{total} ($cm^3\ g^{-1}$)	V_{micro} ($cm^3\ g^{-1}$)
Mn(III)P-CMP	325	143	0.512	0.225
Fe(III)P-CMP	296	115	0.545	0.196
T(p-Br)PPMnCl	16	2.048	2.275×10^{-4}	—

S_{BET}: total BET; S_{micro}: micropore BET; V_{total}: total pore volume; and V_{micro}: micropore volume.

At 77 K, Mn(III)P-CMP displayed a typical type-II and S-type sorption isotherm curve along with a strong adsorption at low pressures ($P/P_0 < 0.1$) (Fig. 2a and c), suggesting the coexistence of micro- and mesopores in the framework. Fig. 2b and d also show that there are a large number of micro- and mesopores in the framework. The main pore diameters were about 1.12 nm and 2.58 nm, and the contributions to the pore volume were 32% and 33% respectively. As evidenced by the gentle curve between 1.12 nm and 2.58 nm, the pore size distribution was relatively uniform and the contribution to the pore volume was 12% (Fig. 2b). Except for the pores with the diameter of 1.06 nm, the pore sizes were unevenly distributed (Fig. 2d). The contribution of 1.06 nm-wide pores to the volume was 26%, whereas that of the total micropores (micropore volume: 0.196 $cm^3\ g^{-1}$) was 36%. On the one hand, the pore structures of Mn(III)P-CMP and Fe(III)P-CMP also verified porphyrin polymerization. On the other hand, the pore structures enhanced the surface area of the polymers that also enhanced the porphyrin reactive sites on the surface of polymers during the reaction.

Monomer T(p-Br)PPMnCl had significantly less amount of nitrogen adsorption at the same pressure and did not show strong adsorption at low pressures ($P/P_0 < 0.1$) as compared to Mn(III)P-CMP (Fig. 2e). The BET surface area was only 16.72 $m^2\ g^{-1}$, which mostly belonged to external specific surface area and pore accumulation. Thus, it was a typical non-porous material.

FE-SEM images (Fig. 3a and b) indicated that Mn(III)P-CMP comprised about 0.2–5.0 μm monoliths originating from the overlapping of circular flakes that were about 200–500 nm in diameter. Transition from a molecular level framework to nanoscale layers and further to microscale monoliths attracted significant attention because it was ubiquitous in biological catalytic systems. The columnar structure was accumulated by nanoscale layers of circular porphyrin flakes among which

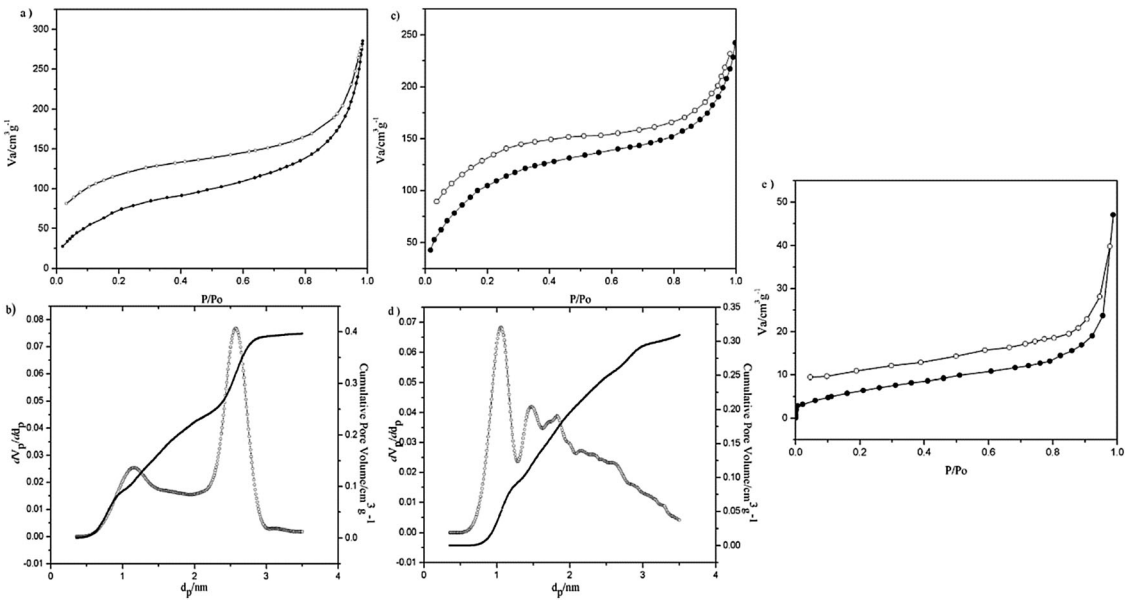

Fig. 2 Nitrogen adsorption (●) and desorption (○) isotherm profiles of MnP-CMP (a), FeP-CMP (c), and T(p-Br)PPMnCl (e) at 77 K; pore size distribution (○) and cumulative pore volume (●) of MnP-CMP (b) and FeP-CMP (d).

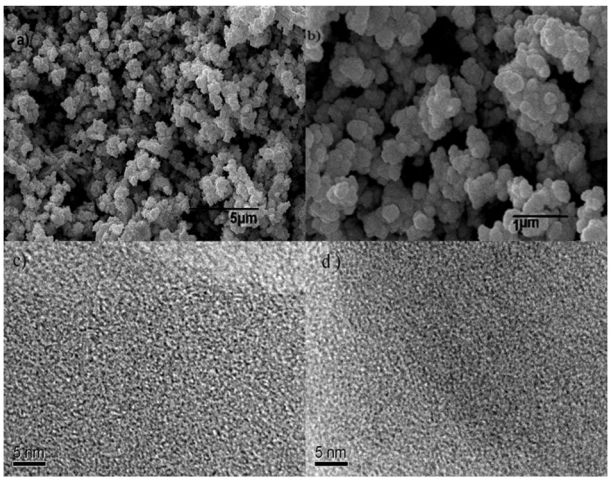

Fig. 3 FE-SEM images of MnP-CMP (a) and FeP-CMP (b); HR-TEM images of MnP-CMP (c) and FeP-CMP (d).

there was network interpenetration. Their surfaces were quite rough and HR-TEM images showed that there were nanopores on the surface of Mn(III)/Fe(III)P-CMP (Fig. 3c and d), consistent with the pore size analysis results. The pore structure and the roughness of the surface implied more reactive site exposure to the substance, which would promote the catalytic reaction.

As shown in Fig. S5 (ESI†), the IR spectrum of T(p-Br)PPMnCl was different from that of Mn(III)P-CMP, which indicates that the reaction occurred on the other side. The characteristic peak at 475 cm^{-1} in the spectrum of T(p-Br)PPMnCl is assigned to C–Br, which attenuates and even disappears in Mn(III)P-CMP due to consumption of C–Br during the coupling reaction. Moreover, Mn(III)P-CMP exhibits a characteristic Mn–N vibration band at 1009.1 cm^{-1}, which is close to that of T(p-Br)PPMnCl (1010.9 cm^{-1}). The bands at 3035 cm^{-1} correspond to the C–H stretches in phenyls, and those at 1516 cm^{-1} and 1608 cm^{-1} correspond to C=C stretches in phenyls. Thus, T(p-Br)PPMnCl had already been introduced into the Mn(III)P-CMP porous structure in which manganese ion was still stably coordinated.

The UV-vis spectrum of Mn(III)P-CMP solid and that of T(p-Br)PPMnCl in $CHCl_3$ solution were also obtained and compared (ESI,† Fig. S6). In the curve, a strong absorption band at 478 nm is the Soret band of T(p-Br)PPMnCl and those at 581 and 618 nm are the Q-bands. Mn(III)P-CMP also shows the same typical UV-vis spectrum as T(p-Br)PPMnCl: there are Soret bands at 462 and 502 nm and Q-bands at 583 and 622 nm. Compared with those in T(p-Br)PPMnCl monomer, the Soret bands in MnP-CMP divide as 462 and 496 nm, belonging to blue- and red-shifted Soret bands of porphyrin, because the conjugate bridge of phenylene increases the molecular connectivity and the electronic coupling in Mn(III)P-CMP, which causes the Soret band to clearly split in Mn(III)P-CMP.[37,38]

The first reduction potential of Mn(III)P-CMP is significantly reduced as compared to that of T(p-Br)PPMnCl (shifts from −0.28 V to −0.12 V) (ESI,† Fig. S7), indicating that phenylene has been introduced into the polymers. As a conjugated bridge between porphyrin monomers, phenylene is advantageous to wide-range flow of electrons and delocalization. As a result, Mn^{3+} ions in the middle of porphyrin rings are further activated and easily form active valence ions Mn^{2+}, thus promoting the catalytic reaction.

The phenylene bridges in four directions of porphyrin rings enable Mn(III)P-CMP to be a highly developed micro- and mesoporous and hyperconjugated metalloporphyrin polymer; hence, the catalytic oxidation activity of Mn(III)P-CMP towards C–H bond is significantly augmented. Furthermore, the XRD profile confirms the amorphous character of Mn(III)P-CMP (ESI,† Fig. S8). Owing to the covalent attachment and cross-linked structure, Mn(III)P-CMP is stable and insoluble in water, dichloromethane, THF, acetone, methanol, DMSO, and some other organic solvents. The thermal property of Mn(III)P-CMP was characterized by thermogravimetric analysis (ESI,† Fig. S9). Mn(III)P-CMP is stable under 300 °C, indicating that Mn(III)P-CMP is highly thermally stable. Accordingly, Mn(III)P-CMP should have excellent catalytic oxidation performance and favorable reusability.

3.2. Catalysis of air oxidation of cyclohexane by Mn(III)P-CMP

To research the catalytic activity and product formation rules of conjugated metalloporphyrin polymers during the air oxidation of cyclohexane, cyclohexane was oxidized with air at 150 °C and 0.8 MPa with Mn(III)P-CMP as the catalyst, and the mixture of reaction products was sampled every 30 min. GC-MS analysis results showed that the main products were cyclohexanol and cyclohexanone, and the by-products were mainly adipic acid, dicyclohexyl adipate, and cyclohexyl hydroperoxide. The contents of cyclohexanone and cyclohexanol analyzed by GC and the contents of adipic acid, ester, and cyclohexyl hydroperoxide measured by chemical titration are shown in Fig. 4. The blank tests showed that cyclohexane could not be oxidized at the same temperature and pressure in the absence of Mn(III)P-CMP and other additives, which indicated that Mn(III)P-CMP acted as a catalyst during cyclohexane oxidation with air. The literature also had a similar blank experimental report.[12]

Changes in the product distribution of cyclohexane oxidation with time are shown in Fig. 4. The catalysis of Mn(III)P-CMP for cyclohexane oxidation with air did not have a significant induction period (Fig. 4a). To explore the reaction mechanism, a radical scavenger, hydroquinone, was added to the reaction system in the initial stage. Since the oxidation reaction hardly occurred, it was a radical type reaction. Moreover, there was a certain amount of cyclohexyl hydroperoxide in the products. Hence, cyclohexyl radical, which was generated *via* the decomposition of cyclohexyl hydroperoxide, was the major active radical in the reaction system. In addition, the mechanism *via* which air oxidation of cyclohexane was catalyzed by Mn(III)P-CMP was similar to that by monomer metalloporphyrin.[39]

The yields of cyclohexanol and cyclohexanone rapidly and linearly increased in the first 3 h. The cyclohexyl hydroperoxide content reached a maximum (2.0%) at 1.5 h and began to gradually decline but remained relatively high at 3 h. As the time further increased, the yields of cyclohexanol and cyclohexanone reached highest (12.8% and 11.5%) at 4 h and 3.5 h, respectively, and plummeted soon afterwards. In the beginning of the reaction,

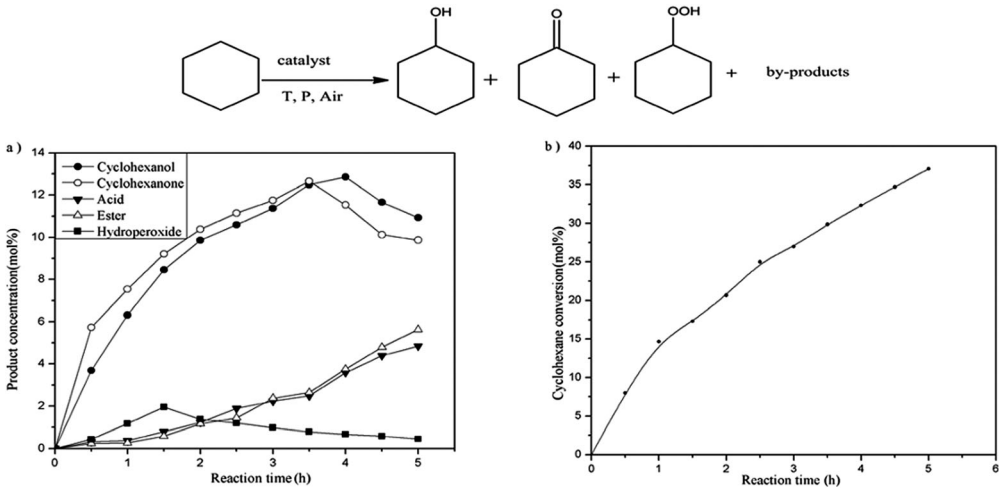

Fig. 4 Cyclohexane conversion and reaction product distribution in the cyclohexane oxidation catalyzed by MnP-CMP; Mn^{3+}/cyclohexane = 1/168 000 (molar ratio), V_{air} = 1000 mL min^{-1}, P = 0.8 MPa, T = 150 °C, and cyclohexane: 200 mL (1.85 mol).

the cyclohexane conversion rate increased faster (Fig. 4b) and then slowed down, reaching 29.9% at 3.5 h, whereas the yields of cyclohexanol and cyclohexanone were maintained at maximum (21.6%). However, at 3 h, white or light yellow solid acid precipitates were produced, and the content and selectivity of alcohol and ketone were lower at the same time, indicating deep oxidation of cyclohexane. Cyclohexane was oxidized with air over Fe(III)P-CMP under the same reaction conditions. The yield of cyclohexanol and cyclohexanone was 19.21%, and that of acid was 1.93%. The conversion of cyclohexane reached 27.51%.

3.3. Effect of reaction temperature on cyclohexane oxidation

Cyclohexane oxidation with air catalyzed by Mn(III)P-CMP was highly sensitive to reaction temperature. The reaction could not take place until the temperature was above 120 °C. The effect of reaction temperature on the product selectivity and cyclohexane conversion rate was evaluated at 135 °C, 140 °C, 145 °C, 150 °C, 155 °C and 160 °C (Table 2 and Fig. 5).

Fig. 5 indicated that the conversion rate of cyclohexane obviously increased as the reaction temperature increased. Moreover, it also showed that the reaction temperature influenced the yields of alcohol and ketone; the higher the temperature, the low the selectivity of cyclohexanol and cyclohexanone. The total content of alcohol and ketone reached maximum at 6 h and 135 °C (Table 2); however, it did not exceed 10.0%. At 140 °C, 145 °C, 150 °C, and 155 °C, the total contents of alcohol and ketone reached maxima at 4.5 h, 4 h, 3.5 h, and 3 h, respectively; the total selectivity ranged from 70.3% to 85%, and the maximum yield of alcohol and ketone was found to be 21.6% at 150 °C. When the temperature was 160 °C, the total contents of alcohol and ketone peaked at 1.5 h. At the same time, the conversion rate of cyclohexane was 26.3%, but the selectivity of oxidation reaction was hardly controllable and the total selectivity of alcohol and ketone was only 66.4%. Moreover, the by-products significantly increased and the reaction system had already generated plenty of acid and ester. As the reaction proceeded, the selectivity of alcohol and ketone sharply dropped to 61.3% at 2 h.

3.4. Comparison of the catalytic activities of the monomer metalloporphyrin and conjugated polymer porphyrin

The aerobic oxidation of cyclohexane catalyzed by Mn(III)P-CMP and Fe(III)P-CMP had higher selectivity and conversion rates than of that catalyzed by T(p-Br)PPMnCl and T(p-Br)PPFeCl, and the results are listed in Table 3 and Fig. 6. The catalysis of cyclohexane oxidation over T(p-Br)PPFeCl with air had a about 0.5 h significant induction period.

In the beginning of the reaction, the conversion rate of cyclohexane linearly increased. Compared with those obtained by Mn(III)P-CMP and Fe(III)P-CMP, the conversion rates of cyclohexane catalyzed by T(p-Br)PPMnCl and T(p-Br)PPFeCl were significantly slower later in the reaction (after 3 h); thus, the catalyst activity had deteriorated by this time. Their catalytic activities followed a descending order of Mn(III)P-CMP > Fe(III)P-CMP > T(p-Br)PPMnCl > T(p-Br)PPFeCl. Alcohol and

Table 2 Effect of reaction temperature on cyclohexane oxidation[a]

Reaction temperature	135 °C	140 °C	145 °C	150 °C	155 °C	160 °C
Reaction time[b] (h)	6.0	4.5	4.0	3.5	3.0	1.5
Cyclohexane conversion (%)	12.5	19.4	21.4	29.9	29.3	26.3
Yields of alcohol and ketone (%)	10.6	14.5	16.0	21.6	18.8	17.5
Catalyst mole TON[c]	21 000	32 592	35 952	50 232	49 224	44 184

[a] Catalyst: Mn(III)P-CMP, Mn^{3+}/cyclohexane = 1/168 000 (molar ratio), V_{air} = 1000 mL min^{-1}, P = 0.8 MPa, and cyclohexane: 200 mL (1.85 mol). [b] Time of maximum (alcohol + ketone) yields. [c] TON was calculated using the following equation: TON = (consumed cyclohexane)/(amount of Mn).

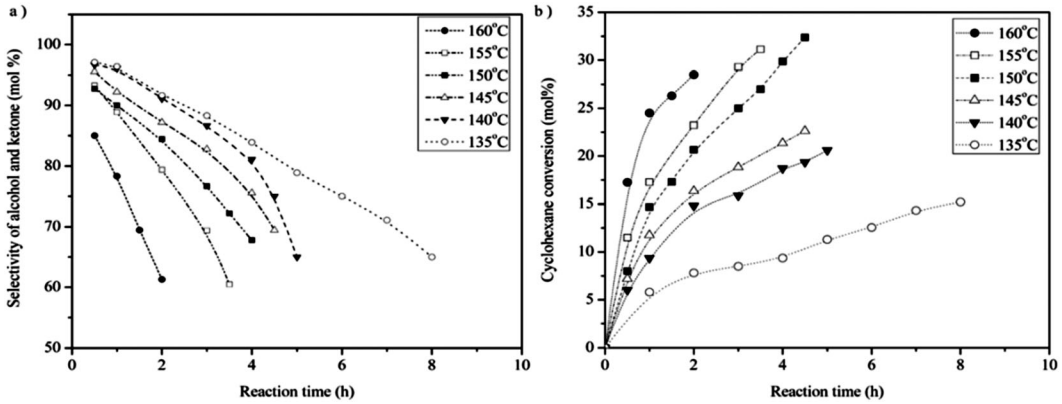

Fig. 5 Selectivity of alcohol and ketone and cyclohexane conversion in the cyclohexane oxidation catalyzed by MnP-CMP at different temperatures; catalyst: MnP-CMP, Mn^{3+}/cyclohexane = 1/168 000 (molar ratio), V_{air} = 1000 mL min^{-1}, P = 0.8 MPa, and cyclohexane: 200 mL (1.85 mol).

ketone were the main products during the porphyrin-catalyzed oxidation of cyclohexane, and there was also a small amount of adipic acid with high economic value. We also compared the conversion rates of cyclohexane as well as the selectivity of alcohol, ketone, and adipic acid at the highest yield of alcohol and ketone (Table 3).

Although the yields of alcohol and ketone reached highest at 3 h with T(p-Br)PPFeCl as the catalyst, they were only 9.4%, which were significantly lower than those of other catalysts. When porphyrin polymer was used as the catalyst, the conversion rate of cyclohexane and the selectivities of alcohol and ketone were elevated by 10% as compared to those obtained by employing monomer metalloporphyrin. The selectivities of alcohol and ketone followed a decreasing order of Mn(III)P-CMP > Fe(III)P-CMP > T(p-Br)PPMnCl > T(p-Br)PPFeCl, *i.e.* porphyrin polymer had significantly higher selectivity than monomer metalloporphyrin. Additionally, the selectivity of porphyrin polymer for adipic acid was obviously lower than that of monomer metalloporphyrin. However, under the same conditions, the conversion rate of cyclohexane catalyzed by porphyrin polymer was higher than that obtained by monomer metalloporphyrin; hence, the yield of adipic acid remained higher.

The developed porous structure and large specific surface area in porphyrin polymer enlarged the contact area between substrate, oxygen, and catalyst; this provided more micro-reaction sites and improved the efficiency of the catalytic reaction. The content of acid in the product slightly increased with the increasing aperture of polymerized porphyrin. Fe(III)P-CMP, whose pore size distribution was mainly concentrated at 1.06 nm, had slightly lower acid selectivity than Mn(III)P-CMP, whose pores were distributed at 1.12 nm and 2.58 nm. Hence, this polymerized porphyrin can improve the selectivity of the main product in the cyclohexane oxidation reaction owing to its unique porous structure and shape-selective effect and make the selectivity of alcohol and ketone less dependent on the conversion rate of cyclohexane, simultaneously maintaining high cyclohexane conversion rate as well as selectivity of alcohol and ketone.

3.5. Reusability of metalloporphyrin polymers

Monomer metalloporphyrin is prone to degradation and inactivation in a homogeneous catalytic oxidation system. At the end of the reaction with Mn(III)P-CMP or Fe(III)P-CMP as the catalyst, the mixture was centrifuged and the supernatant that was detected by UV-vis spectroscopy did not contain metalloporphyrin. The metal leaking experiment was also performed. The filtrate obtained after fifth reaction cycle was tested by atomic absorption spectrometry using a Perkin Elmer analyst 700/800. The concentration of Mn in the filtrate was 1.14×10^{-5} mg mL^{-1} and it was about 0.4% of the amount in the original solution (3.0×10^{-3} mg mL^{-1}) (Mn^{3+}/cyclohexane = 1/168 000). Moreover, 87% of Mn(III)P-CMP catalyst was recovered by centrifugation, filtration, and thorough washing with THF, methanol, and trichloromethane in the fifth recovery experiment. Thus, it can be seen that the loss mostly occurred in the recovery process

Table 3 Influence of different catalysts on the cyclohexane oxidation reaction[a]

Reaction temperature	T(p-Br)PPFeCl	T(p-Br)PPMnCl	Fe(III)P-CMP	Mn(III)P-CMP
Reaction time[b] (h)	3.0	3.5	4.0	3.5
Cyclohexane conversion (%)	15.6	19.2	27.5	29.9
Selectivity of alcohol and ketone (%)	60.2	62.3	69.8	72.3
Selectivity of adipic acid (%)	17.0	18.8	7.0	8.9
Yields of alcohol and ketone (%)	9.4	11.9	19.2	21.6
Yields of adipic acid (%)	2.6	3.6	1.9	2.7
Catalyst mole TON[c]	20 267	24 895	46 200	50 232

[a] Catalyst: M^{3+}/cyclohexane = 1/168 000 (molar ratio), V_{air} = 1000 mL min^{-1}, T = 150 °C, P = 0.8 MPa, cyclohexane: 200 mL (1.85 mol). [b] Time of maximum (alcohol + ketone) yields. [c] TON was calculated using the following equation: TON = (consumed cyclohexane)/(amount of Mn/Fe).

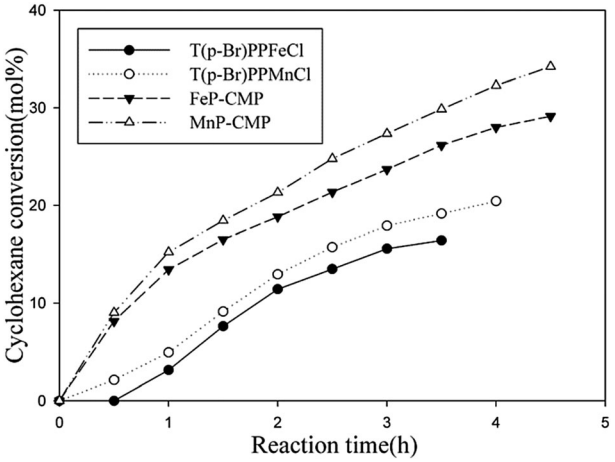

Fig. 6 Cyclohexane conversion in the cyclohexane oxidation catalyzed by MnP-CMP, FeP-CMP, T(p-Br)PPMnCl, and T(p-Br)PPFeCl; M^{3+}/cyclohexane = 1/168 000 (molar ratio), V_{air} = 1000 mL min^{-1}, T = 150 °C, P = 0.8 MPa, and cyclohexane: 200 mL (1.85 mol).

rather than in the reaction process. For example, some catalysts adhered on the filter membrane.

Metalloporphyrins connected by coupling reaction with phenyls effectively prevented the metalloporphyrin moiety from being oxidized, improving its stability. After recycling for 5 times, the BET surface area of the recovered Mn(III)P-CMP was still up to 300 m^2 g^{-1}, close to the initial value (325 m^2 g^{-1}). The SEM images of the catalysts used were nearly same as those of the original material with rough circular flakes structure (ESI,† Fig. S11). The EDX test (Fig. S12, ESI†) of Mn(III)P-CMP and Fe(III)P-CMP showed that the relative contents of elements remained almost unchanged after repeated use. Hence, they had excellent catalytic properties and repeatability due to their large surface areas and porous structures. Particularly, the conversion rate of cyclohexane exceeded 25% after Mn(III)P-CMP was recycled 5 times, which only dropped by less than 5% as compared to the first conversion rate (ESI,† Fig. S13). Moreover, the total selectivity of cyclohexanol and cyclohexanone hardly changed. Similarly, the conversion rate of cyclohexane exceeded 23% after Fe(III)P-CMP was used 5 times. Reduction of industrial costs by continuing to increase the recycle time is potentially applicable in industry.

4. Conclusions

Using tetraphenylporphyrin as the raw material, we synthesized new metalloporphyrin-conjugated polymers (Mn(III)P-CMP and Fe(III)P-CMP) to apply metalloporphyrin in heterogeneous catalysis, prevent it from oxidation damage, and allow recycling in the oxidation reaction. These polymers were stable such that they did not dissolve or decompose in common solvents even at high temperatures. With large surface areas and porous structures, Mn(III)P-CMP and Fe(III)P-CMP had the specific surface areas of up to 325 m^2 g^{-1} and 296 m^2 g^{-1}, respectively, and the contributions of micropore to the pore volume were 44% and 36%, respectively. Cyclohexane was oxidized with air over MnP-CMP at the Mn^{3+}/cyclohexane molar ratio of 1/168 000 and air flow rate of 1000 mL min^{-1}. The total yield of cyclohexanol and cyclohexanone was 21.6%, and the conversion of cyclohexane reached 29.9%. In addition, polymer porphyrin had a recovery rate of over 87%. After being recycled 5 times, the conversion rates of cyclohexane exceeded 25% and 23% when Mn(III)P-CMP and Fe(III)P-CMP were used, respectively. By realizing heterogeneous catalysis, metalloporphyrin-conjugated polymers can replace the corresponding metalloporphyrin for industrial catalytic oxidation and thus have significant application prospects.

Acknowledgements

The financial support of the National Natural Science Foundation of China (Grant No. 21576074) is gratefully acknowledged. We are also grateful for the financial support of Hunan University.

References

1 A. M. Kirillov, M. V. Kirillova and A. J. L. Pombeiro, *Adv. Inorg. Chem.*, 2013, **65**, 1–31.
2 S. Gupta, M. V. Kirillova, M. F. C. Guedes da Silva, A. J. L. Pombeiro and A. M. Kirillov, *Inorg. Chem.*, 2013, **52**, 8601–8611.
3 S. S. P. Dias, M. V. Kirillova, V. Andre and A. M. Kirillov, *Inorg. Chem.*, 2015, **54**, 5204–5212.
4 U. Schuchardt, D. Cardoso, R. Sercheli, R. Pereira, R. S. da Cruz, M. C. Guerreiro, D. Mandelli, E. V. Spinace and E. L. Pires, *Appl. Catal., A*, 2001, **211**, 1–17.
5 J. Rittle and M. T. Green, *Science*, 2010, **330**, 933–937.
6 P. R. O. de Montellano and J. J. De Voss, in *Cytochrome P450: structure, mechanism, and biochemistry*, ed. P. R. O. de Montellano, Kluwer Academic/PlenumPublishers, New York, 2005, pp. 183–245.
7 J. C. Barona-Castaño, C. C. Carmona-Vargas, T. J. Brocksom and K. T. de Oliverira, *Molecules*, 2016, **21**, 310.
8 K. S. Suslick, in *The Porphyrin Handbook*, ed. K. M. Kadish, K. M. Smith and R. Guilard, Academic Press, New York, 2000, pp. 41–60.
9 T. A. Moore, D. Gust, P. Mathis, J. C. Mialocq, C. Chachaty, R. V. Bensasson, E. J. Land, D. Doizi, P. A. Liddell, W. R. Lehman, G. A. Nemeth and A. Moore, *Nature*, 1984, **16**, 630–632.
10 B. Meunier, *Chem. Rev.*, 1992, **92**, 1411–1456.
11 U. Besmar, J. B. Lyon and F. J. MiIIer, *US Pat.*, 4720592, 1988.
12 C. C. Guo, M. F. Chu, Q. Liu, Y. Liu, D. C. Guo and X. Q. Liu, *Appl. Catal., A*, 2003, **246**, 303–309.
13 C. C. Guo, X. Q. Liu, Y. Liu, Q. Liu, M. F. Chu and X. B. Zhang, *J. Mol. Catal. A: Chem.*, 2003, **192**, 289–294.
14 M. J. Nappa and C. A. Tolman, *Inorg. Chem.*, 1985, **24**, 4711–4719.
15 M. Moghadam, S. Tangestaninejad, M. H. Habibi and V. Mirkhani, *J. Mol. Catal. A: Chem.*, 2004, **217**, 9–12.
16 Y. Yan, P. P. Yao, Q. Mu, L. Wang, J. Mu, X. Q. Li and S. Z. Kang, *Appl. Surf. Sci.*, 2011, **258**, 58–63.

17 M. Wei, J. M. Wan, Z. W. Hu, Z. Q. Peng and B. Wang, *Appl. Surf. Sci.*, 2016, **377**, 149–158.
18 H. J. Mackintosh, P. M. Budd and N. B. Mckeown, *J. Mater. Chem.*, 2008, **18**, 573–578.
19 G. Huang, J. Luo, C. C. Deng, Y. A. Guo, S. K. Zhao, H. Zhou and S. Wei, *Appl. Catal., A*, 2008, **338**, 83–86.
20 K. S. Suslick, P. Bhyrappa, J. H. Chou, M. E. Kosal, S. Nakagaki, D. W. Smithenry and S. R. Wilson, *Acc. Chem. Res.*, 2005, **38**, 283–291.
21 Z. Wang, S. W. Yuan, A. Mason, B. Reprogle, D. J. Liu and L. P. Yu, *Macromolecules*, 2012, **45**, 7413–7419.
22 H. J. Mackintosh, P. M. Budd and N. B. McKeown, *J. Mater. Chem.*, 2008, **18**, 573–578.
23 P. Kaur, J. T. Hupp and S. T. Nguyen, *ACS Catal.*, 2011, **1**, 819–835.
24 T. Hasell, C. D. Wood, R. Clowes, J. T. A. Jones, Y. Z. Khimyak, D. J. Adams and A. I. Cooper, *Chem. Mater.*, 2010, **22**, 557–564.
25 R. W. Wagner, T. E. Johnson and J. S. Lindsey, *J. Am. Chem. Soc.*, 1996, **118**, 11166–11180.
26 A. M. Shultz, O. K. Farha, J. T. Hupp and S. T. Nguyen, *Chem. Sci.*, 2011, **2**, 686–689.
27 N. B. McKeown, S. Hanif, K. Msayib, C. E. Tattershall and P. M. Budd, *Chem. Commun.*, 2002, 2782–2783.
28 A. I. Cooper, *Adv. Mater.*, 2009, **21**, 1291–1295.
29 J. X. Jiang, F. B. Su, A. Trewin, C. D. Wood, N. L. Campbedd, H. J. Niu, C. Dickinson, A. Y. Ganin, M. J. Rosseinsky, Y. Z. Khimyak and A. I. Cooper, *Angew. Chem.*, 2007, **46**, 8574–8579.
30 P. E. Ellis and J. E. Lyons, *J. Chem. Soc., Chem. Commun.*, 1989, **16**, 1187–1188.
31 L. Chen, Y. Yang and D. L. Jiang, *J. Am. Chem. Soc.*, 2010, **132**, 9139–9145.
32 L. Chen, Y. Yang, Z. Q. Guo and D. L. Jiang, *Adv. Mater.*, 2011, **23**, 3149–3154.
33 Y. J. Li, B. S. Sun and W. J. Yang, *Appl. Catal., A*, 2016, **515**, 164–169.
34 Y. J. Li, B. S. Sun, Y. R. Zhou and W. J. Yang, *Appl. Organomet. Chem.*, 2017, **31**, 170–176.
35 A. D. Alder, F. R. Long and F. K. Kampos, *J. Inorg. Nucl. Chem.*, 1970, **32**, 2443–2445.
36 W. W. Kaeding, R. O. Lindblom, R. G. Temple and H. I. Mahon, *Ind. Eng. Chem. Process Des. Dev.*, 1965, **4**, 97–101.
37 A. Satake and Y. Kobuke, *Org. Biomol. Chem.*, 2007, **5**, 1679–1691.
38 N. Aratani and A. Osuka, *Org. Lett.*, 2001, **3**, 4213–4216.
39 J. E. Lyons, P. E. Ellis and H. K. Myers, *J. Catal.*, 1995, **155**, 59–73.

